Final Draft
of the original manuscript:

Li, Y.; Angelova, A.; Hu, F.; Garamus, V.; Peng, C.; Li, N.; Liu, J.; Liu, D.; Zou, A.:

pH Responsiveness of Hexosomes and Cubosomes for Combined Delivery of Brucea javanica Oil and Doxorubicin.

In: Langmuir. Vol. 35 (2019) 45, 14532 - 14542.
First published online by ACS: October 22, 2019

DOI: 10.1021/acs.langmuir.9b02257
https://doi.org/10.1021/acs.langmuir.9b02257

pH-Induced Inverted Hexagonal-to-Cubic Phase Transition in Dual Drug Loaded Lyotropic Liquid Crystalline Carriers of *Brucea Javanica Oil* and Doxorubicin

Yawen Li[a], Angelina Angelova[b], Fangzhou Hu[a], Vasil M. Garamus[c], Changjun Peng[a], Na Li[d], Jianwen Liu[a], Dan Liu[a], Aihua Zou[a*]

[a]*Shanghai Key Laboratory of Functional Materials Chemistry, State Key Laboratory of Bioreactor Engineering and Institute of Applied Chemistry, School of Chemistry and Molecular Engineering, East China University of Science and Technology, Shanghai 200237, P. R. China*

[b]*Institut Galien Paris-Sud, CNRS UMR 8612, Univ. Paris-Sud, Université Paris-Saclay, LabEx LERMIT, F-92296 Châtenay-Malabry cedex, France,*

[c]*Helmholtz-Zentrum Geesthacht, Centre for Materials and Coastal Research, D-21502 Geesthacht, Germany*

[d] *National Center for Protein Science Shanghai and Shanghai Institute of Biochemistry and Cell Biology, Shanghai 200237, P. R. China*

[*]To whom correspondence should be addressed.

Tel/Fax: +86-21-64252231

E-mail: aihuazou@ecust.edu.cn

†East China University of Science and Technology.

ABSTRACT

We report pH-responsive liquid crystalline lipid nanoparticles, which are dual loaded by *Brucea javanica* oil (BJO) and doxorubicin hydrochloride (DOX) and display a pH-induced inverted hexagonal (pH=7.4) to cubic (pH≤6.8) phase transition with a therapeutic application in cancer inhibition. *Brucea javanica* oil is a traditional herbal medicine that strongly inhibits the proliferation and metastasis of various cancers. Doxorubicin is an anti-tumor drug, which prevents DNA replication and hampers protein synthesis through intercalation between the base pairs of the DNA helices. Its dose-dependent cardiotoxicity imposes the need of safe delivery carriers. Here pH-induced changes in the structural and interfacial properties of designed multicomponent drug delivery (monoolein-oleic acid-BJO-DOX) systems are determined by synchrotron small-angle X-ray scattering (SAXS) and the Langmuir film balance technique. The nanocarrier assemblies displayed good physical stability in the studied pH range and adequate particle sizes and zeta potentials. Their interaction with model lipid membrane interfaces was enhanced under acidic pH conditions, which mimic the microenvironment around tumor cells. *In vitro* cytotoxicity and apoptosis studies with BJO-DOX dual-loaded pH-switchable liquid crystalline nanoparticles (BJO-DOX-LCNPs) were performed with the human breast cancer MCF-7 cells line and MCF-7 cells with doxorubicin resistance (MCF-7/DOX), respectively. The obtained pH-sensitive nanomedicines demonstrated enhanced anti-tumor efficacy. The performed preliminary studies suggested a potential reverse of the resistance of the MCF-7/DOX cells to DOX. These results highlighted the necessity of further understanding of the link between the established pH-dependent drug release profiles of the nanocarriers and the role of their pH-switchable inverted hexagonal, bicontinuous cubic, sponge or emulsified emulsion inner organizations for the therapeutic outcomes.

KEYWORDS: lyotropic liquid crystalline nanoparticles, pH-responsiveness, synchrotron SAXS, surface pressure/area isotherms, multidrug delivery, human breast cancer MCF-7 cells apoptosis

INTRODUCTION

Tolerance of cancer cells to drugs during chemotherapy is a serious obstacle to cancer treatment.[1-3] The sensitivity of cancer cells to chemotherapeutic drugs gradually decreases with the progress of chemotherapy, which results in multidrug resistance (MDR).[1] Currently, natural products and phytochemicals are attracting growing interest in the design of anticancer medicines including nanoscale assemblies.[4-6] The development of nano-drug delivery systems for cancer therapy aims at maximizing the anticancer drug bioavailability and efficacy, whilst reducing the toxicity associated with conventional chemotherapy formulations.[7-10] New ideas about design and fabrication of nano-drug carriers have arisen from the colloidal properties of liquid crystalline assemblies suitable for incorporation of anti-tumor agents.[11-22] In recent years, liquid crystalline lipid nanocarriers have found applications in various research fields: from biosensors and theranostic imaging in medicine to functional foods, nutraceuticals and drug delivery systems in therapeutic innovation.[23-28] Such carrier systems protect the therapeutic molecules from degradation, provide drug transport and sustained release as well as efficient uptake by the cells.[23,24] Their structures often mimic some naturally occurring complex fluid systems.[7] Major advantages of them are the large surface area-to-volume ratio and the inner organization involving lipid bilayers (hydrophobic compartments) and a network of hydrophilic aqueous channel compartments for accommodation of guest molecules of various origins.[4,16,17]

Lipid-based liquid crystalline assemblies display stimulus-responsive properties (temperature, magnetic field, light, or their combinations)[29-38] of interest in treatment of pathological states. Among them, pH-switchable drug delivery nanocarriers support the triggered release of bioactive compounds into the cytoplasm of cells.[35-37]

The purpose of the present work is to design and characterize dual-drug loaded novel pH-responsive lyotropic liquid crystalline nanoparticles for the combined delivery of phytochemical (BJO) and chemotherapeutic (DOX) drugs towards more efficient cancer cell inhibition.

The seed oil of *Brucea javanica* (BJO), extracted from *Brucea javanica* (Linnaeus) plant, is a traditional herbal medicine with antitumor activity.[39-49] The main bioactive components of BJO are oleic acid, linoleic acid, tetracyclic triterpene quassinoids and anthraquinone.[39] It has been reported that BJO can induce apoptosis through both the mitochondrial pathway and the death receptor pathway.[40] BJO can arrest the cell cycle in the G0/G1 phase and inhibit the cell growth. Moreover, it can reverse the drug resistance in tumor cells by altering the P-glycoprotein expression in the cell membranes.[41-45] The emulsion formulation BJOE has been clinically used in China to treat several carcinoma types including lung cancer, prostate cancer, and gastrointestinal cancer.[45-48] However, the BJOE formulation is thermodynamically unstable owing to phase separation events.[47] In oral administration, BJO is not supported by the patients because of its smell. Therefore, alternative drug delivery systems (liposomes, nanostructured lipid carriers (NLC) or polymer particles)[48] have to be envisioned for BJO encapsulation in order to improve its absorption and bioavailability. The pH-responsiveness of BJO-loaded nanoformulations has not been previously investigated.

Doxorubicin hydrochloride (DOX) is a widely used anthracycline for treatment of various cancers, hematological malignancies, soft tissue sarcomas, and solid tumors.[50] Nevertheless, the limited penetration and distribution and the inherent multidrug resistance of solid tumors to DOX have resulted in the failure of the free drug.[38] It has been suggested that the combination of BJO and DOX may effectively treat malignant hydrocele and succeed to reverse the resistance of cancer cells to DOX.[49]

Considering the bioactivity and the physico-chemical properties of the BJO and DOX drugs, we propose to combine them in self-assembled nanocarriers with the purpose to reach an improved therapeutic outcome and overcome the existing limitations of their bioavailability. Here, we show that the self-assembled organizations of the obtained pH-responsive nanoparticles correspond to different liquid crystalline structures under the pH environment of normal and cancer cells. The pH-sensitivity of the nanocarriers is due to (i) the oleic acid fraction of the lipid phase and (ii) the BJO ingredient, which contains unsaturated fatty acids. We investigated

the effect of the drug content of the nanoparticles in addition to the pH effect. Synchrotron SAXS measurements were performed in order to identify the pH-switchable liquid crystalline types and the corresponding structural parameters, which determine the drug release characteristics. The Langmuir monolayer film technique was used to probe the pH sensitivity of the interfacial properties of the investigated lipid systems. The controlled-release features of the nanocarriers and their biological effects were studied using the human breast cancer MCF-7 cell line model.

EXPERIMENTAL SECTION

Materials. Brucea javanica seed oil (BJO) was received from Yan'an Changtai Pharmaceutical Co., Ltd. (China). Information from the supplier indicated that BJO comprises 63.3 wt.% oleic acid. Glycerol monooleate (MO) was obtained from General-Reagent Co. Ltd. (China). Pluronic F-127 was provided by BASF (Germany). Doxorubicin hydrochloride (DOX) and oleic acid (OA) were purchased from Aladdin Chemical Reagent Co. Ltd. (China). 1,2-dipalmitoyl-sn-glycero-3-phosphocholine (DPPC) was a product of Avanti Polar Lipids (USA). Fetal bovine serum, DMEM medium, 3-(4,5-dimethylthiazol-2-yl)-2,5-diphenyltetrazoliumbromide (MTT), and 4',6-diamidino-2-phenylindole (DAPI) were purchased from Boster Co. Ltd. (China). All materials were used as received without further purification. The water used in the experiments was double distilled.

Sample preparation. Lyotropic liquid crystalline nanoparticles (LCNPs) with pH sensitivity were prepared with the top-down technique.[8] Table 1 presents the compositions employed for the preparation of the self-assembled LCNPs based on the nonlamellar lipid monoolein (MO) and the BJO-loaded pH-sensitive nanocarriers (BJO-LCNPs). As BJO itself contains OA, the oleic acid (OA) content in the mixed lipid systems was gradually varied with increasing the BJO content. The initial ratio of MO to OA was chosen based on the pH-dependence of the protonation state of the OA structures.[31, 32] The ratio MO/OA was kept constant by decreasing the OA amount

when increasing the quantity of encapsulated BJO. Briefly, the lipid phase containing MO, OA and BJO and the Pluronic F127 polymer stabilizer were mixed and melted at 60 ^{o}C in order to prepare a homogeneously mixed blend. Subsequently, a pre-heated PBS buffer was added to the lipid/F127 blend and further intensely stirred at 10000 rpm for 10 min. The obtained dispersions were processed through a high-pressured homogenizer (HPH ATS Engineering, Canada) with five homogenization cycles at 600 bars.

Table 1 Compositions of pH-sensitive lyotropic liquid crystalline nanoparticles systems. The mixed assemblies were prepared by partially replacing oleic acid (OA) by BJO in the shown sequence. The commercial BJO drug contains 63.3% OA. The numbers in the sample codes MO-0.9OA-0.1BJO, MO-0.8OA-0.2BJO, MO-0.7OA-0.3BJO, MO-0.6OA-0.4BJO, and MO-0.5OA-0.5BJO correspond to the proportions of OA and BJO with regard to the total OA in the samples. The total fraction of OA is taken as 1.

Sample codes[a]	**MO/g**	**OA/g**	**BJO/g (OA_{BJO}/g)**	**OA_T/g**	**F127/g**	**Aq. phase PBS/ml**
MO-OA	3.60	2.40	-	2.40	0.60	54.00
MO-0.9OA-0.1BJO	3.60	2.16	0.38 (0.34)	2.40	0.61	57.01
MO-0.8OA-0.2BJO	3.60	1.92	0.76 (0.48)	2.40	0.63	58.09
MO-0.7OA-0.3BJO	3.60	1.68	1.14 (0.72)	2.40	0.64	59.68
MO-0.6OA-0.4BJO	3.60	1.44	1.52 (0.96)	2.40	0.66	61.00
MO-0.5OA-0.5BJO	3.60	1.20	1.90 (1.20)	2.40	0.67	62.08

[a]OA_T is the total amount of oleic acid in the system.

OA_T=OA+OA_{BJO}, where OA_{BJO} means the amount of oleic acid in the commercial BJO.

All experiments were performed using an aqueous phase of phosphate buffer saline (a PBS buffer containing 98 mM NaCl and 30 mM phosphate buffer). The pH values

were adjusted by the addition of 1M NaOH and 1M HCl. The doxorubicin hydrochloride (DOX) drug was dissolved in the PBS buffer phase at the corresponding concentration and used for the preparation of dual DOX-BJO loaded pH-sensitive liquid crystalline nanoparticles (DOX-BJO-LCNPs) based on the same method. The concentrations of DOX in the cell culture texts were varied between 0 and 50 μg/ml at a constant BJO concentration (200 μg/ml).

Particle size and zeta potential. The mean particle sizes, polydispersity index (PDI) and zeta potentials of the samples were characterized by dynamic light scattering (DLS) using a Delsat Nano C Particle Analyzer (Beckman Coulter, USA). Prior to analysis, the samples were diluted with PBS (1/10, v/v) to avoid multiple scattering effect, which may be caused by high turbidity. The measurements were performed at a fixed angle of 165° and at 25 ^{o}C. The equilibration time for pH adjustment in the dispersions was one hour before the measurements.

Small-angle X-ray scattering (SAXS) experiments. Small-angle X-ray scattering (SAXS) experiments were performed at the beamline BL19U2 of the National Center for Protein Science Shanghai (NCPSS) at the Shanghai Synchrotron Radiation Facility (SSRF). The X-ray radiation wavelength λ, was 1.033 Å. The scattered X-ray intensities were measured using a Pilatus 1M detector (DECTRIS Ltd). The sample-to-detector distance in the SAXS experiments was set so that the detecting momentum transfer q [$q = 4\pi \sin\theta/\lambda$, where 2θ is the scattering angle] was in the range from 0.01 to 0.5 Å^{-1}. A flow cell made of a cylindrical quartz capillary with a diameter of 1.5 mm and a wall of 10 μm was used. The exposure time of 1-2 seconds provided no radiation damage. The X-ray beam size 0.40× 0.15 (H x V) mm^2 was adjusted to pass through the center of the capillary in every measurement. Ten images were acquired for each sample and buffer in order to obtain a high signal-to-noise ratio. The 2D scattering images were converted into 1D SAXS curves through an azimuthal averaging after a solid angle correction. Then, they were normalized with the intensity of the transmitted X-ray beam using the software package BioXTAS RAW.

Entrapment efficiency (EE) and drug loading (DL). The free DOX drug was

separated from the drug entrapped in the DOX-BJO-LCNPs by using the ultrafiltration centrifugal method.[17] Briefly, the nanoparticles dispersion was diluted 10 times and centrifuged for 40 min at 8000 rpm using centrifugal filter tubes (MWCO = 10 kDa; Millipore, USA) at 4℃. The particles were separated from the aqueous phase and the free drug was analyzed in the supernatant. The UV-Vis spectrophotometric method was used to measure the free drug concentration in the samples after centrifugation and supernatant collection. The absorption measurements were performed at a wavelength 233 nm using a UV-Vis spectrophotometer UV-1800 (Shimadzu, Japan). The experiments were performed at room temperature (25 ^{o}C).

The EE and DL results were calculated using the equations (1) and (2):

$$\mathrm{EE\%} = \left(1 - \frac{C_F}{C_T}\right) \times 100\% \quad (1)$$

$$\mathrm{DL\%} = \left(\frac{C_T - C_F}{C_L}\right) \times 100\% \quad (2),$$

where C_T, C_F, and C_L are the total amount of DOX present in the dispersion system, the amount of non-entrapped DOX, and the total amount of lipids, respectively.

***In vitro* release of DOX.** The *in vitro* release of DOX from DOX-BJO-LCNPs was investigated by the dialysis method.[48] A freshly prepared DOX-BJO-LCNPs dispersion was placed into a dialysis tube with 14kDa MW cutoff. The latter was incubated in release media (i) PBS, pH 7.4; 150 mL, (ii) PBS, pH 6.8; 150 mL and (iii) PBS, pH=5.4 at temperature 37 ◦C under rotary shaking. In addition, the release of the pure drug DOX at PBS, pH 7.4; 150 mL was used as control. Aliquot samples (4 mL) were taken out from the release medium at pre-determined time points and the system was refilled with the same volume of fresh medium. Subsequently, the DOX content was determined at a wavelength 233 nm by means of a UV-vis spectrophotometer (UV-1800, Shimadzu, Japan).

Langmuir film balance. Surface pressure *versus* molecular area isotherms were recorded using the Langmuir mini-trough (KSV NIMA, Finland) equipped with

hydrophilic barriers. A force transducer connected to an alloy wire probe with a sensitivity of ±0.01 mN/m was used as a surface pressure sensor. The surface pressure was recorded as a function of the molecular area in experiments controlled by the KSV NIMA LB software. The phospholipid DPPC was studied as a lipid membrane model. DPPC was dissolved in chloroform and spread at the air/water interface. The system was left for 30 min for solvent evaporation. The temperature was kept constant at 20±0.5 °C. Different concentrations of DOX-BJO-LCNPs (0, 0.25, 0.5 mg/L) were added to the aqueous subphase in order to study the concentration effect of DOX-BJO-LCNPs interaction with lipid monolayers at varying pH values. The monolayer compression was accomplished at a barrier speed of 10 mm/min. The monolayers spread on pure water subphase or on a solution of DOX-BJO-LCNPs (0.5 mg/L) were compressed to a target surface pressure (5 and 35mN/m) with a rate of 10 mm/min. Then, the monolayer relaxation was recorded at a constant molecular area as surface pressure *versus* time (π-t) plots.

***In vitro* cellular cytotoxicity assays.** The Michigan Cancer Foundation-7 (MCF-7) human breast cancer cell line was purchased from the American Type Culture Collection (ATCC CCL-185, Manassas, VA, USA). The cells were seeded into cell culture dishes containing DMEM medium supplemented with 10% fetal bovine serum and 1% penicillin at 37 ◦C in a humidified 5% CO_2 atmosphere.

MTT assay was performed to evaluate the cytotoxicity of the dual-drug loaded DOX-BJO-LCNPs. Human breast carcinoma MCF-7 cells were plated in 96-well plates with 100 μL medium at a density of 5×10^3 cells per well. After 24h, the growth medium was removed and the cells were exposed to various concentrations of blank-LCNPs, free drug BJO, free drug DOX, a combination of BJO and DOX, and DOX-BJO-LCNPs for 24h. Then, the culture medium was discarded and replaced with a fresh medium containing 0.5mg/ml MTT. After incubation for another 4 h at 37ºC, the resulting formazan crystals were solubilized with 100 μL DMSO. The absorbance was measured using a microplate reader at a wavelength 492 nm, with the absorbance at 630 nm as the background correction. The effect of the nanoparticle formulations on the cell proliferation was expressed as the cell viability percentage.

Untreated cells were considered as 100% viable. The calculation of the IC_{50} value (50% inhibiting concentration) was done by using the GraphPad Prism for Windows.

Cell apoptosis assays. The MCF-7 cells were plated in 6-well plates at a density of 1×10^4 cells per well. After 24 h, the cells were exposed to blank-LCNPs, free drug BJO, free drug DOX, or DOX-BJO-LCNPs (20μg/mL of DOX) for 24 h. Then, a solution of DAPI (5μg/mL) was added and incubated for 15 min at room temperature after washing the cells with cold PBS buffer. The excess dye was removed by cold PBS buffer twice. The cells were fixed with paraformaldehyde. The stained cells were imaged under a fluorescent microscope ECLIPSE Ti-S (Nikon, Japan) in order to study the cell apoptosis.

RESULTS AND DISCUSSION

Phase behavior and pH-responsiveness of BJO-loaded liquid crystalline nanoparticles

Dispersions of liquid crystalline lipid nanoparticles (LCNPs) with and without encapsulated BJO were prepared by the top-down technique. The encapsulation efficiency of BJO in all samples was above 96%. In the LCNPs formulations, the commercial oil-phase drug BJO was gradually replaced by OA (Table 1). Thus, all samples contain oleic acid (OA), which can change its protonation state at different pH values. It has been suggested that the pH of the environment influences the critical packing parameter of fatty acid-containing lipid mixtures.[31, 32] As a consequence, the variations of pH may lead to changes in the supramolecular structures, which display pH-sensitive properties.

The structural organizations of the samples described in Table 1 were investigated by means of synchrotron SAXS in the pH range between 1.5 and 8. The obtained SAXS patterns are shown in Figure 1. The liquid crystalline phase type was identified by indexing of the resolved Bragg peak positions.[51] The patterns of the drug-loaded MO-OA-BJO samples were compared with the known liquid crystalline phases of the

self-assembled MO-OA systems lacking BJO.[32,33] This allowed examining the pH sensitivity of the liquid crystalline structures in the presence and in the absence of encapsulated BJO drug.

An inverted hexagonal (H_{II}) phase was observed for the MO-OA system at pH=7.4 with relative positions of the Bragg peaks spaced at 1, √3 and √4. The estimated lattice parameter of the H_{II} phase is a_H=6.89nm. The decrease of pH yielded disappearance of the Bragg peaks of the hexosome nanocarriers. A cubic (*Pn3m*) liquid crystalline phase was identified at pH 6.8 as the main structure. For the diluted dispersion of lipid nanocarriers, the first three Bragg peaks of the cubic structure were well distinctive and spaced in the ratio 1, √2, √3, and √4. A minor fraction of the *Im3m* cubic phase seems also be present. It is favoured by the inclusion of the Pluronic F127 stabilizer.

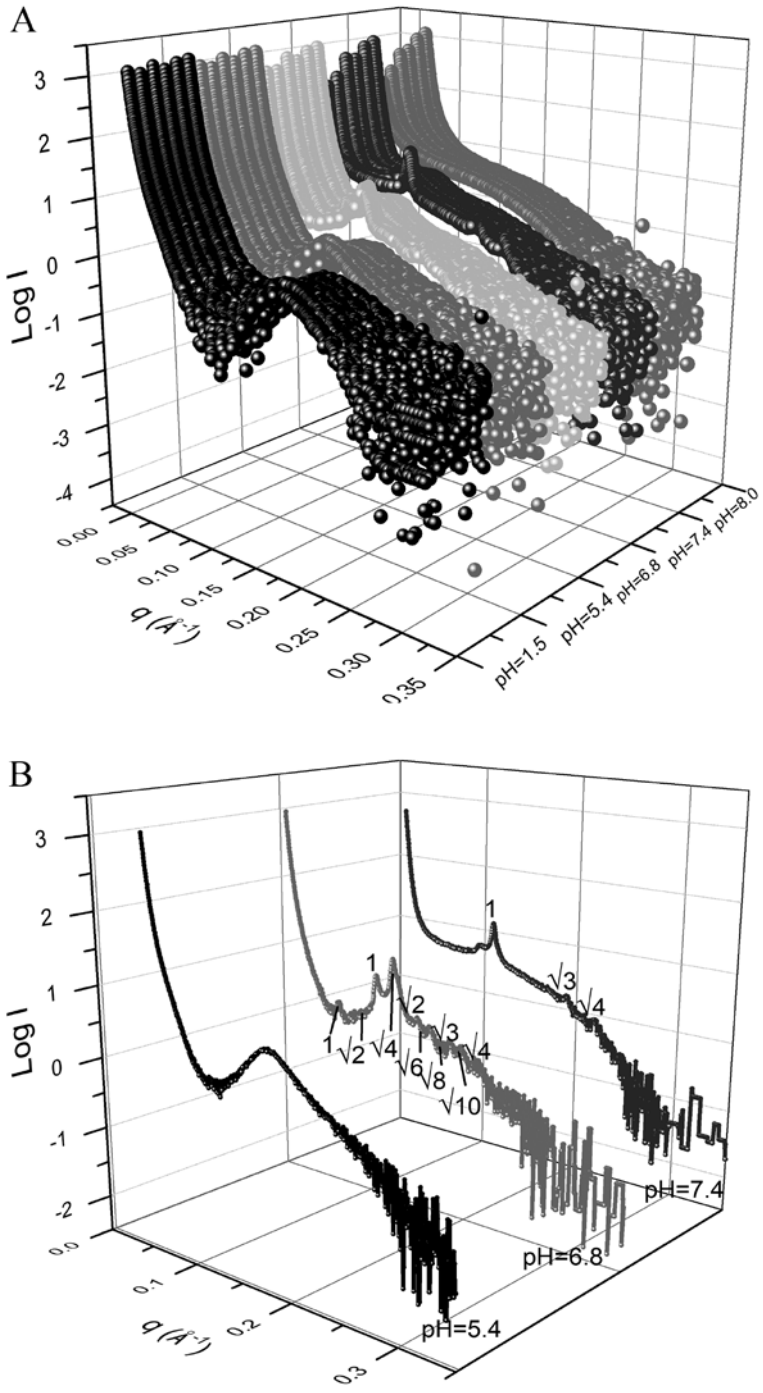

Figure 1. (A) SAXS patterns of pH-sensitive lyotropic liquid crystalline nanocarriers as a function of the pH values of the aqueous environment. Six compositions (MO-OA, MO-0.9OA-0.1BJO, MO-0.8OA-0.2BJO, MO-0.7OA-0.3BJO, MO-0.6OA-0.4BJO and MO-0.5OA-0.5BJO) (in the order from front to back) are presented for each pH value: pH=1.5, pH=5.4, pH=6.8, pH=7.4 and pH=8.0. (B) Indexing of the Bragg peaks of the inverted hexagonal (H_{II}) (pH 7.4) and the inverted cubic (pH 6.8) liquid crystalline phases for the BJO-containing nanocarriers MO-0.9OA-0.1BJO is shown together with the pattern recorded at pH 5.4 and corresponding to a sponge phase or an emulsified microemulsion (EME).

The SAXS profiles of the nanoparticles recorded at high and low pH values did not exhibit periodic-types of liquid crystalline organizations (Figure 1). The membrane curvature resulting from the homogeneous mixing of the ingredients in the self-assembled mixtures at pH=8 corresponded to a sponge-like assembly.[4,19] In the case of acidic pH=1.5 and 5.4 conditions, broad maxima were observed in the SAXS patterns indicating that the long range order diminished. This is characteristic also for sponge phase nanocarriers or emulsified microemulsions (EME).[31,52,53] The SAXS results in Figure 1 confirm the pH sensitivity of the nanocarriers structures, which are formed at the fully protonated state of OA. Evidently, OA influences the interfacial hydration state of the lipid bilayers. Despite of the pH sensitivity of the supramolecular organizations, the periodic liquid crystalline structures gradually disappears with the increase of the BJO content. This is due to the oil-type nature of the BJO drug, which increases the fluidity of the MO lipid membranes and hampers their crystallization. The MO-0.9OA-0.1BJO system was subsequently chosen for further investigations in order to maintain a more ordered liquid crystalline type structure of the nanocarriers.

The particle sizes of the dispersed MO-OA-BJO samples were less than 200 nm, and with low PDI values, as determined by DLS. Table S1 shows the differences in the particle sizes under different pH conditions. This fact also confirms the pH sensitivity of the studied nanocarrier dispersions.

Characterization of dual-drug loaded (DOX-BJO) pH-sensitive liquid crystalline nanoparticles

The compositions of the dual-drug loaded (DOX-BJO) nanocarriers were optimized with the help of MTT experiments (see Supporting Information). The cell viability measurements permitted to determine the combinations of DOX and BJO concentrations, which yielded higher toxicity to MCF-7 cancer cells. Various

experiments (determination of drug encapsulation efficiency (EE), nanoparticle sizes, zeta-potentials, and cumulative in vitro drug release) were performed in order to find out the optimal amount of the DOX drug to be encapsulated together with BJO in pH-sensitive liquid crystalline nanoparticles (LCNPs).

Three dual-drug loaded formulations (DOX:BJO=1:40, 1:20, and 1:10) were selected as representative for further investigations based on the obtained data for nanocarriers stability, particle sizes, PDI, and drug entrapment efficiency. Figure 2 shows the results of the physico-chemical characterizations by DLS and the values of the entrapment efficiency determined with the chosen compositions on day 1, day 15 and day 30, respectively.

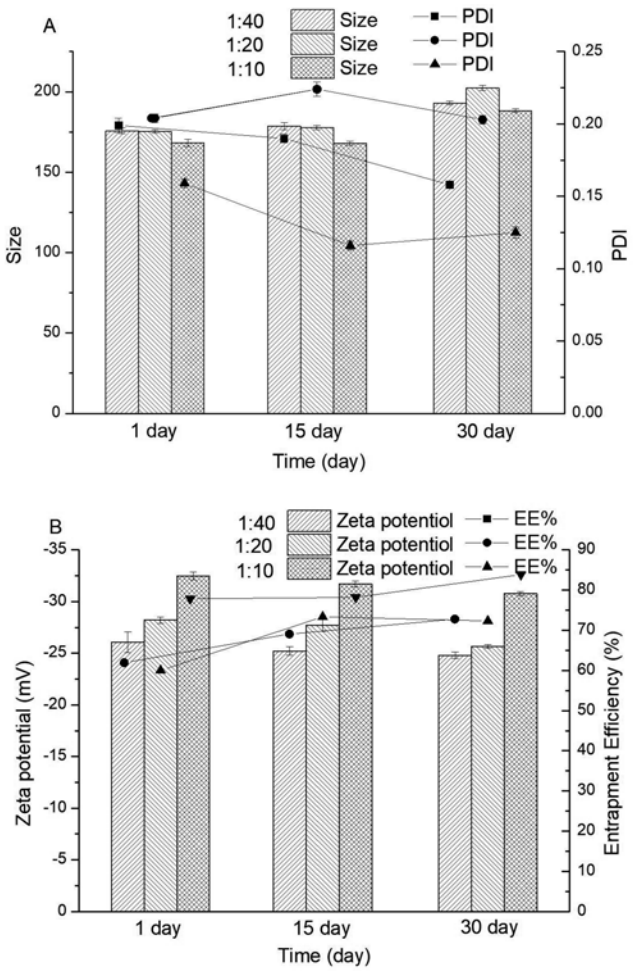

Figure 2. Physico-chemical characterization of the nanocarriers by DLS and DOX entrapment efficiency in DOX-BJO-LCNPs (drug ratios DOX:BJO=1:40, 1:20, 1:10) at 1 day, 15 days and 30 days after the preparation.

As shown in Figure 2 the particle sizes, PDI and zeta-potentials of the selected dual-drug loaded nanocarriers remain almost unchanged during 30 days. The particle sizes of all samples were smaller than 200 nm and the PDI values were low. It should be noted that the surface charge is an indication for the electrostatic stabilization of the colloidal nanoparticles system. The repulsion between nanoparticles with the same sign of the surface charge contributes to enhanced stability. Moreover, steric stabilization is provided by the Pluronic stabilizer, which helped for the dispersion of the lipid nanoparticles in the medium. The zeta-potential values presented in Figure 2 indicated negative charges on the LCNPs surfaces, which are due to the deprotonation of OA.[31] The zeta potential modulus showed a slight decrease after 30 days of storage, but the absolute zeta potential values of all samples were higher than 25mV. This fact proved the stability of the prepared LCNPs upon storage.

The encapsulation efficiency (EE) values of DOX reached high values of 60%-77% for the freshly prepared samples (Figure 2). DOX appeared to be efficiently encapsulated into the nanochannel organization of the studied liquid crystalline carriers. The storage time of 30 days maintained elevated encapsulation efficiency. The DOX-BJO-LCNPs carrier system with a drug ratio DOX: BJO=1:10 (denoted as the DOX:BJO=1:10 sample) was chosen for further investigations based on the results about particle sizes, zeta potentials and encapsulation efficiencies.

Synchrotron SAXS investigations were performed to determine the inner organization of the designed dual-drug (DOX-BJO) loaded nanocarriers. Representative SAXS patterns, before and after DOX loading in the BJO-LCNPs are shown in Figure 3. Our study established that the nanoparticles undergo a pH-induced structural switch of their inner liquid crystalline organizations. Hexosomes carriers (with an inner H_{II}-phase structure) are formed at pH=7.4, whereas cubosomes carriers (with coexisting *Pn3m*/*Im3m* inner cubic structures) are formed at pH=6.8.

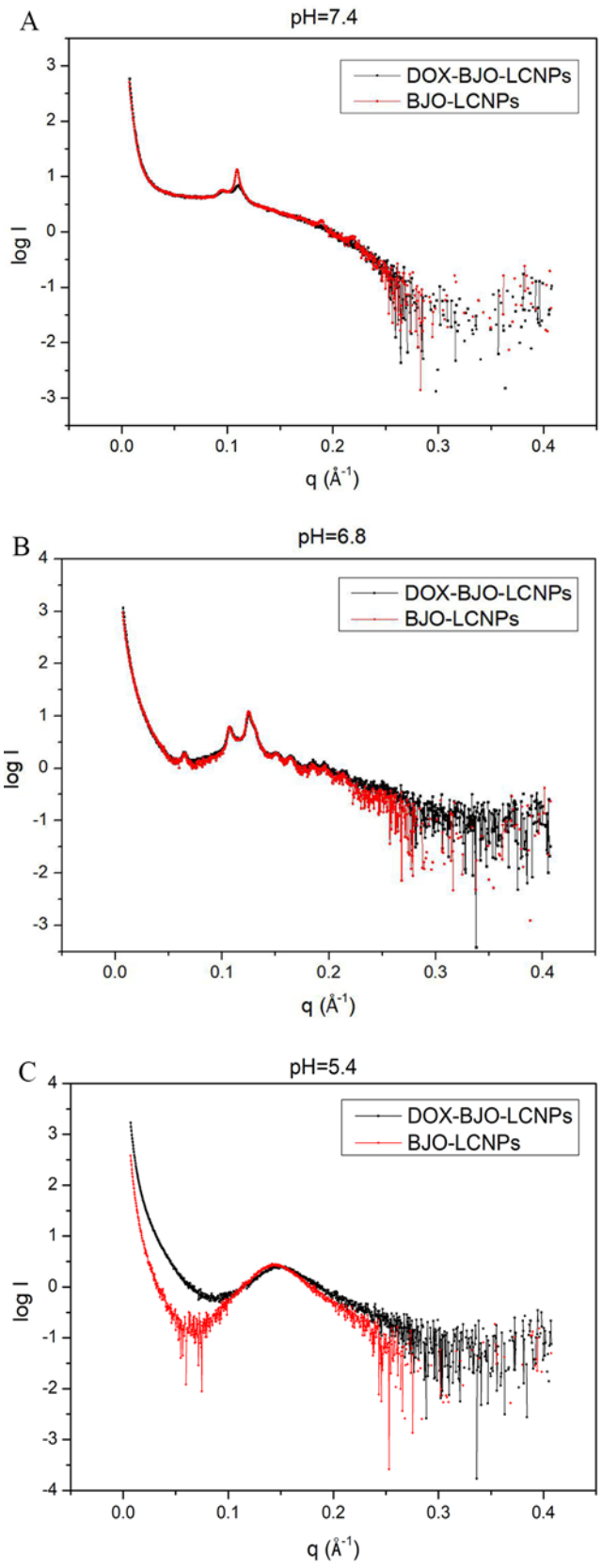

Figure 3. Comparison of the SAXS patterns of DOX-BJO-LCNPs and BJO-LCNPs at different pH values 7.4, 6.8 and 5.4. The lipid ratio is MO-0.9OA-0.1BJO. The drug ratio after loading of DOX in the BJO-LCNPs is DOX:BJO=1:10.

Figure 3 reveals that the pH-sensitivity of the scattering curves is more pronounced upon DOX encapsulation in the LCNPs systems. The obtained SAXS plots show that the internal liquid crystalline structures of the drug-loaded carriers (DOX-BJO-LCNPs) are preserved after DOX encapsulation. However, the Bragg peaks intensity of the DOX-BJO LCNPs dispersions decreases at pH 7.4. The shift of the correlation peaks bumps may correspond to larger distances and lower ordering upon loading of DOX. At pH 5.4, the correlation peak of the DOX-loaded carriers became narrower. These structural data evidence the successful encapsulation of the DOX molecules in the nanostructures. Correspondingly, the structural parameters of the host carrier system are modified. This conclusion is supported also by the direct determination of the DOX encapsulation efficiency in the nanoparticles.

The SAXS results suggest that the DOX-BJO-LCNPs may take an advantage of the existing pH differences in the extracellular tumor microenvironment[54] because the obtained LCNPs structures reflect a pH-induced switch. Hence, the pH-dependent structures of the nanocarriers may be exploited towards potential tumor treatment. It is known that there is weak acidity around the tumor cells (about pH 6.8) as compared with the normal cell environment (physiological pH=7.4),[54] whereas the pH of intracellular lysosome and endosomes in tumor cells is around 5.4.

The release profiles of DOX from the DOX-BJO-LCNPs are shown in Figure 4 at different pH values. The release of DOX from a pure-drug suspension was investigated as a control. Figure 4 demonstrates that more than 90% of DOX was rapidly released from the pure drug suspension within 6h. The DOX-BJO-LCNPs formulations showed smooth release curves at pH=7.4, pH=6.8 and pH=5.4. No burst release was observed. Compared to the samples with liquid crystalline structures (pH=7.4 and pH=6.8), the release rate of the drug from the sponge (or EME samples) at pH=5.4 was significantly faster. Besides, we established that the release rate of DOX from the DOX-BJO-LCNPs formulation at pH=7.4 was slower than that at pH=6.8. This different sustained release behavior corroborates with the SAXS results about the presence of different LCNPs structures (inverted hexagonal or cubic phases)

under the different pH conditions. According to previous reports, drugs encapsulated in host cubic phases are released easier as compared to the release from a hexagonal phase.[33,34,55] Drug diffusion from lyotropic liquid crystalline carriers is dependent on the topology and the diameters of the water channels in the internal structure. In agreement with previous reports,[56] drug release from the bicontinuous cubic phase network of large open channels is more rapid than that from hexagonally packed channels of smaller diameters. The obtained here sustained release results for DOX-BJO-LCNPs reveal a slowest rate of drug release in the simulated normal cell (pH=7.4) physiological environment, a faster release rate in the simulated external tumor cell environment (pH=6.8), and a maximal rate in the simulated intracellular lysosome environment (pH=5.4). This effect may reduce the cytotoxicity of DOX for healthy cells and facilitate the efficacy of the drug in the pathological state.

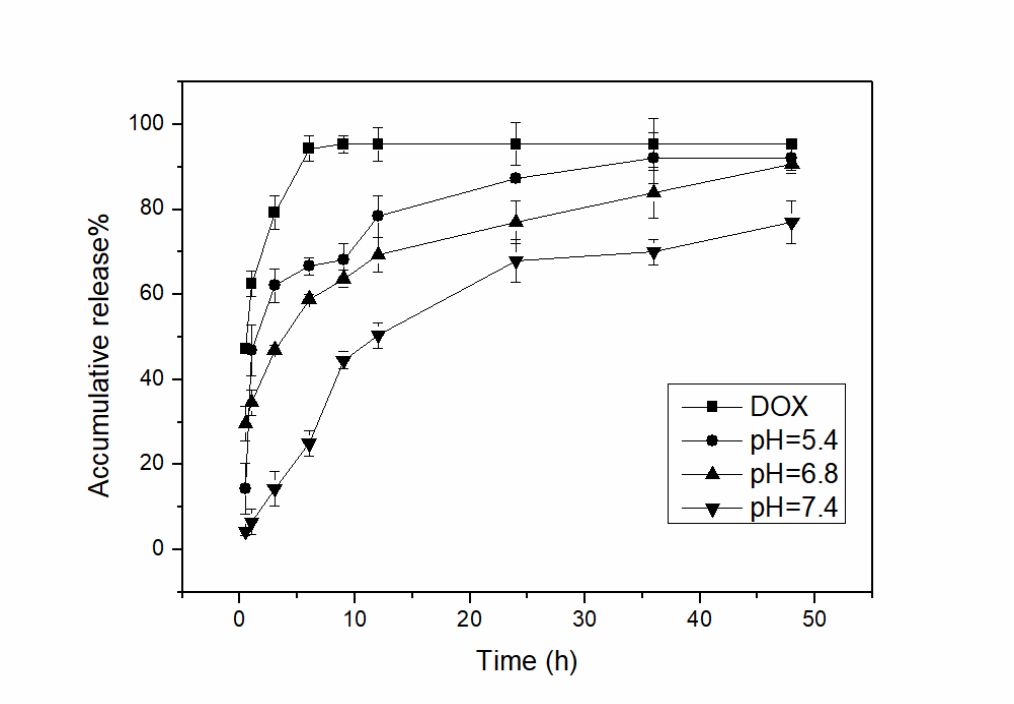

Figure 4. Cumulative *in vitro* release of DOX from DOX-BJO-LCNPs or a suspension of a free drug (control) in a release medium of PBS (pH=7.4, pH 6.8 or pH 5.4) at 37ºC. All values are expressed as a mean ± SD (n=3). According to the performed SAXS analysis, the internal structures of the DOX-BJO-LCNPs correspond to hexosomes (formed at pH=7.4), cubosomes (formed at pH=6.8), and spongosomes or EMEs (formed at pH=5.4).

Interaction of liquid crystalline nanoparticles with lipid membrane interfaces

Phospholipid monolayers and bilayers are used as models of biological membranes when studying the effects of drugs and drug carriers on the biomembrane properties.[57-61] We used the Langmuir film technique to examine the interfacial behavior of different liquid crystalline structures (cubic or hexagonal phase nanoparticles resulting from the pH sensitivity of the studied systems) on DPPC phospholipid monolayers.

Surface pressure *versus* area isotherms were recorded with phospholipid DPPC monolayers on pure water subphase and on solutions of DOX-BJO-LCNPs (Figure 5). The concentration range of the DOX-BJO-LCNPs (0, 0.25, 0.5 mg/L) was chosen following the outcome of the experiments presented in the Supporting Information.

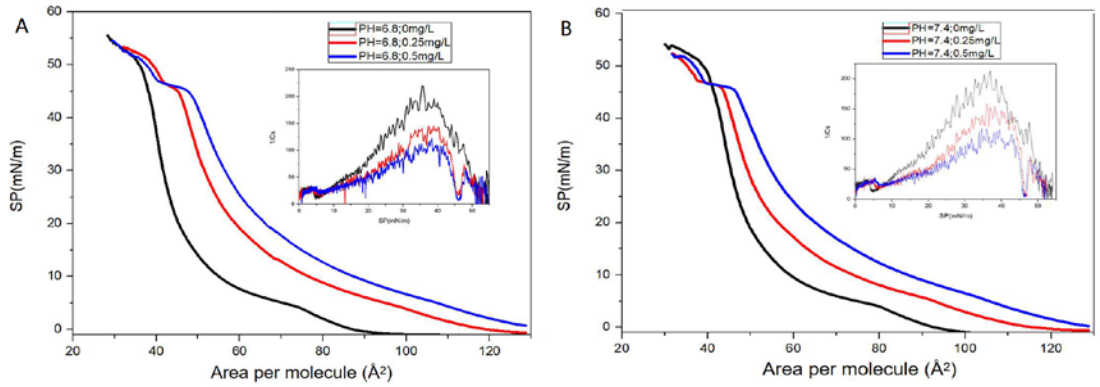

Figure 5. Surface pressure *vs* area per molecule isotherms (π/A isotherms) of DPPC (a phospholipid membrane model) on subphases containing increasing concentrations of DOX-BJO-LCNPs at pH=6.8 (A) and 7.4 (B). Inset: Compression modulus *vs* surface pressure plots.

The interfacial behavior of the DOX-BJO-LCNPs upon interaction with DPPC monolayers at pH values 7.4 and 6.8 is characterized by the π/A isotherms in Figure 5. The model lipid membranes show increased mean molecular areas in their isotherms, which correspond to DPPC monolayer expansion at increasing concentrations of the DOX-BJO-LCNPs in the aqueous subphase. The pH effects on the interfacial adsorption of the LCNPs are compared, through the π/A isotherms, for the inverted

hexagonal phase liquid crystalline structures (at pH 7.4) and the cubic phase liquid crystalline particles (at pH 6.8). The changes in the lift-off area, A_L, at which the surface pressure starts to rise above the zero baseline level in the π/A curves, indicated that the drug-encapsulating nanocarriers penetrate into the DPPC monolayers at low surface pressures. The area A_L (Table S2) increases significantly with the increase of the nanocarrier concentration in the subphase of constant pH. The collapse pressure (π_c) and the mean molecule area at the collapse pressure (A_c) did not show significant differences with the variation of the DOX-BJO-LCNPs concentration. This suggested that the drug carriers are squeezed from the interface into the subphase beneath the monolayers when they are compressed to high surface pressures. Because there was no obvious phase transition process in the isotherm of the monolayer during compression, the phase state of the monolayer cannot be judged directly from the isotherm, so it need to be determined according to the compression modulus. At constant pH, the compression modulus of the DPPC monolayers decreased significantly with the increase of the concentration of the drug carriers in the subphase (Figure 5 inset). The surface pressure required for the transition of the lipid monolayer from a liquid expanded (LE) state to a liquid condensed (LC) film state increased essentially upon interaction with LCNPs. The results imply that the adsorption of the drug carriers hinders the formation of the LC phase in the model lipid membrane.

The effect of the fixed drug carrier concentration on the π-A isotherm of the DPPC monolayers at different pH values of the aqueous subphase is presented in Figure S3. The studied liquid crystalline structures resulted in different degrees of expansion of the DPPC monolayers. The interfacial monolayer expansion degree was maximal at pH 6.8, *i.e.* at the pH causing a structural switch to a cubic inner organization of the dual-drug loaded carriers.

The interfacial behavior of the DOX-BJO-LCNPs upon interaction with DPPC monolayers was examined at a constant pressure. The relaxation of the DPPC monolayers was monitored at applied surface pressures of 5 mN/m and 35 mN/m (corresponding to the LE and LC phase states of the monolayers, respectively) at LCNPs concentration 0.25mg/L, 0.5 mg/L and at different pH values of the subphase

(Figure 6). The purpose was to better understand the effect of the drug carriers on the stability of the DPPC monolayers at the air/water interface.

The obtained π *vs.* time plots suggested that the relative increase in surface pressure of the cubic phase nanocarriers (pH 6.8) was much more pronounced for DPPC monolayers precompressed to 5 mN/m. This meant at pH=6.8 the nanoparticles were more easily adsorbed at low pressure. While at the liquid condensed phase (35 mN/m), which state was close to the normal cell membrane, the the nanocarriers of inverted hexagonal liquid crystalline structures (pH 7.4) retained less on the membrane and were more easily squeezed from the monolayers.Therefore, they interact more weakly with the model lipid membrane. The interaction with the lipid film interface was enhanced at acidic pH, which causes a switch to cubosomes structures.[61-64]

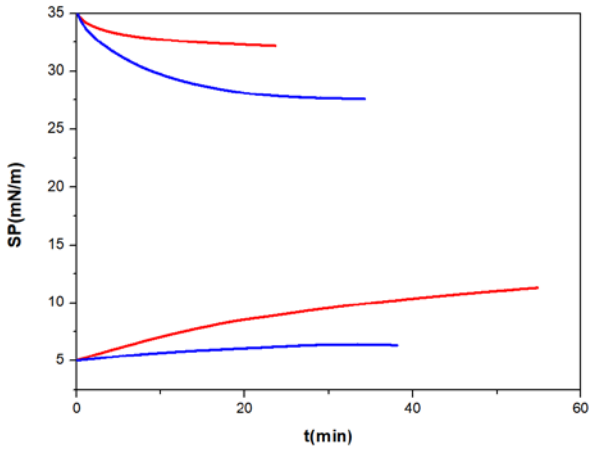

Figure 6. Surface pressure *vs.* time (π-t) curves at pH=6.8 (red) and pH 7.4 (blue) at a drug carrier concentration 0.5mg/L.

Based on the above, it can be concluded that the interfacial interaction between the DOX-BJO-LCNPs with the model lipid membranes appears to be stronger for the case of the cubic phase (cubosome) nanocarriers at pH 6.8. Considering the established pH sensitivity of the liquid crystalline carriers and the pH-induced structural transformations, it can be expected that the interactions of the DOX-BJO-LCNPs with the cancer cells will be more pronounced under acidic pH

conditions (corresponding to the pH of simulated tumor microenvironment).[54] The DLS results in Figure 2 showed small sizes of the drug delivery assemblies, which should be beneficial for their cellular uptake.

Biological evaluations of the dual-drug loaded nanocarriers with human breast carcinoma MCF-7 cells

The cytotoxicity of the studied drug delivery nanocarriers DOX-BJO-LCNPs to human MCF-7 tumor cells as well as to cells selected for resistance against doxorubicin (MCF-7/DOX) was evaluated using an MTT assay. Figure 7 presents the results of the viability of the MCF-7 carcinoma cells at different compositions of the formulations. The viability of the MCF-7 cells treated for 24h with combined BJO-DOX formulations, which contain 3.12 μg/mL and 50 μg/mL DOX, was (75.8±2.2)% and (38.6±1.9)%, respectively. The cytotoxicity of the DOX-BJO-LCNPs against MCF-7 cells at concentrations of DOX ranging from 3.12 to 50 μg/mL was significantly higher than that of the non-encapsulated BJO-DOX mixture. This may be due to the sustained release properties of the DOX-BJO-LCNPs, which are characterized by prolonged release profiles (Figure 4). Moreover, Figure 7A shows that the DOX-BJO-LCNPs nanosystem exhibits the highest inhibition potential among all formulations and anti-cancer apoptotic effects in the studied concentration range. These data suggest that the DOX-BJO-LCNPs had an advantage of tumor cell killing over the pure drugs. The blank nanocarriers did not show any obvious cytotoxicity to the MCF-7 cells. Evidently, the drug uptake by the tumor cells is considerably higher from the DOX-BJO-LCNPs formulation. Thus, the outcome of the MTT assay demonstrates that the efficacy of the DOX and BJO drugs is augmented upon encapsulation in nanocarriers as compared to the bioactivity of the free drugs. In parallel, the toxicity of DOX-BJO-LCNPs to MCF-7 cells at pH=6.8 and 7.4 was also studied. At low drug concentrations, the cellular toxicity at pH=6.8 was slightly higher, but the difference was not obvious when the concentration increased (Figure S4).

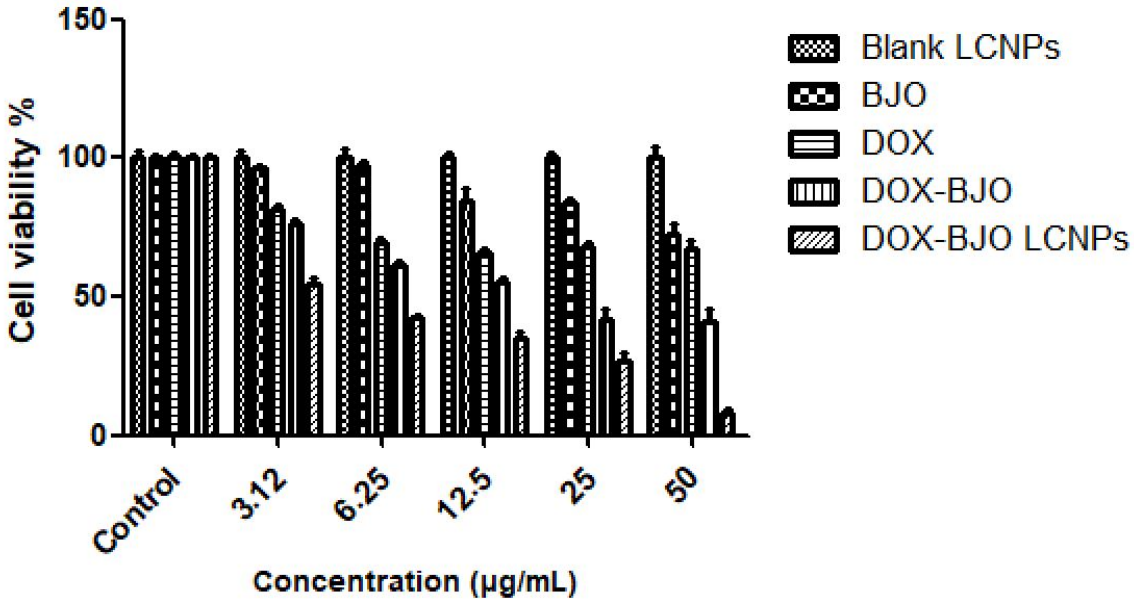

Figure 7. *In vitro* cytotoxicity of BJO, DOX, DOX-BJO and DOX-BJO-LCNPs formulations to human breast carcinoma MCF-7 cells for 24 h. Cell viability is expressed as the percentage of untreated controls. Data are given as mean ± SD (n = 5). For the DOX-BJO-LCNPs with a DOX:BJO=1:10 ratio, the investigated corresponding concentrations of the pure drug BJO and BJO in DOX-BJO-LCNPs were 10 times higher than the indicated DOX concentrations (µg/ml). The concentration of the blank carriers (LCNPs) was consistent with that of the corresponding drug-loaded carriers.

Apoptotic studies were performed in order to determine the initial cell death occurring with MCF-7 cancer cells exposed to DOX-BJO-LCNPs *versus* free drugs (Figure 8). After incubation with the DOX-BJO-LCNPs formulation, the MCF-7 cells were stained with the fluorescent dye DAPI, which is suitable for analysis of living cells undergoing apoptosis. The results indicated that the MCF-7 cells were intact in the control sample (Figure 8A). Tumor cells incubated with the blank LCNPs showed the same state as the control group, which evidenced that the blank LCNPs did not cause cell apoptosis (Figure 8B). On the other hand, the suspension of the two drugs DOX-BJO and the DOX-BJO LCNPs effectively induced apoptosis (Figure 8C, D). Preliminary results about DOX-BJO-LCNPs reverse of the resistance of the MCF-7/DOX cells to DOX are presented in Supporting Information (Figure S5).

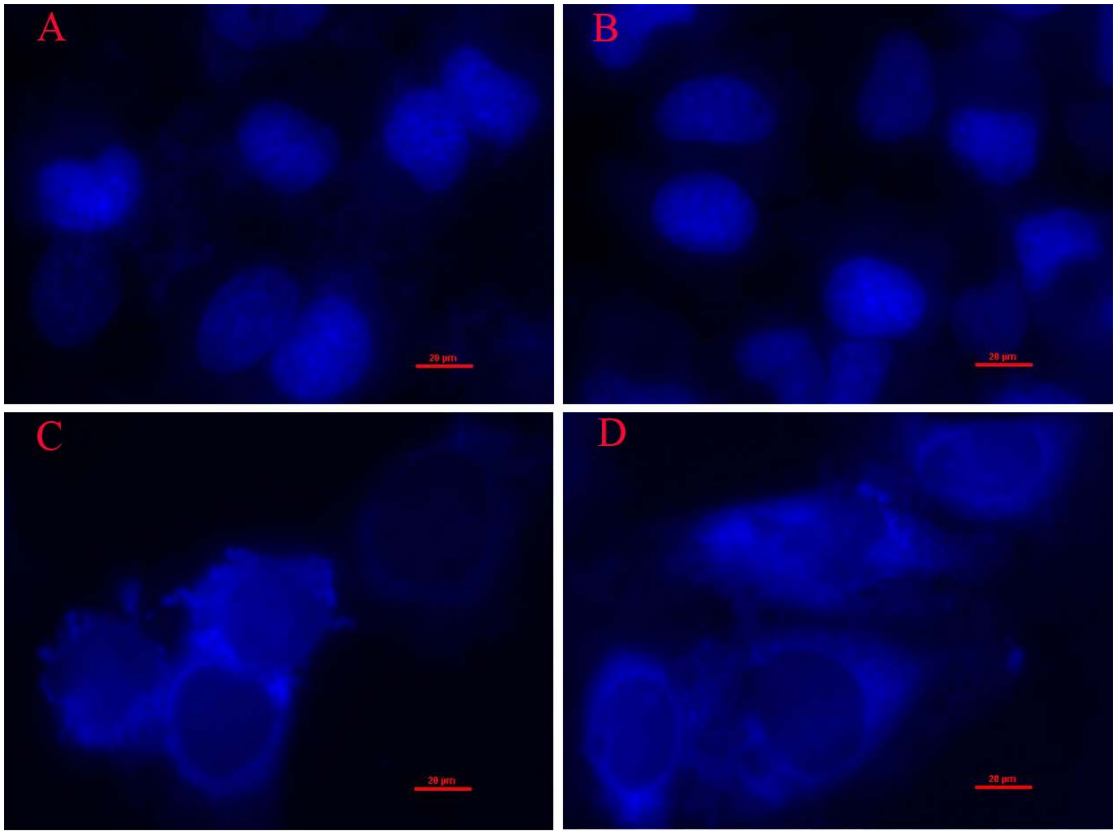

Figure 8. Effect of different formulation treatments on the apoptotic behavior of MCF-7 cancer cells. A: Control; B: Blank lipid nanocarriers; C: dual-drug loaded DOX-BJO LCNPs; D: DOX-BJO suspension.

CONCLUSION

pH-sensitive liquid crystalline nanoparticles loaded with BJO were successfully formulated thanks to the pH-dependent ionization state of OA. The lyotropic lipid liquid crystalline carriers co-encapsulated two drugs with different solubilities and bioactivities (a phytochemical (BJO) and a chemotherapy agent (DOX)). The optimized DOX-BJO-LCNPs formulation showed long-term stability, high encapsulation efficiency, and controlled drug release properties. The Langmuir film balance experiments indicated that the designed cubosome nanocarriers interact stronger with the lipid membrane interface under acidic conditions, which mimic the cancer cells microenvironment. *In vitro* cytotoxicity and apoptosis studies of

DOX-BJO-LCNPs with the human MCF-7 carcinoma cells demonstrated an enhanced anti-tumor effect. This signifies that the dual drug-loaded carriers appear to be more efficient in their anti-cancer apoptotic effects in comparison to the suspension of the free drugs. Moreover, the pH-responsive DOX-BJO-LCNPs drug delivery system can be expected to reverse the resistance of the MCF-7/DOX cells to DOX. The established structural transitions and physicochemical properties should be exploited in future biological experiments on combination anti-cancer therapy with dual-drug loaded nanoparticles. The pH-induced phase change from an inverted hexagonal liquid crystalline structure (pH=7.4, simulated normal cell environment) to cubic network architectures of open channels (pH < 6.8, simulated weakly acidic pH environment around cancer cells), and more weakly organized sponge or microemulsion phases (pH=5.4, simulated acidic endosome/lysosome environment inside cancer cells) can be correlated with the sustained drug release properties of the novel LCNPs.

ASSOCIATED CONTENT

Supporting information

Figures with additional results for hydrodynamic particle sizes of MO-OA-BJO samples; determination of the ratio between DOX and BJO for preparation of DOX-BJO-LCNP carriers; π-A isotherms of DPPC monolayers interacting with DOX-BJO-LCNPs at different concentrations; determination of A_L, A_∞, π_c and A_c of DPPC monolayers spread on a subphase of DOX-BJO-LCNPs; viability MTT assay at pH=6.8 and pH=7.4; viability MTT assay of DOX-BJO-LCNPs on MCF-7/DOX cells, and microscopy imaging of apoptosis.

AUTHOR INFORMATION

Corresponding Author

aihuazou@ecust.edu.cn

Funding Source

This work was supported by the National Natural Science Foundation of China (Grants No. 21573070, 21872051, U1832144).

Notes

The authors declare no competing financial interest.

ACKNOWLEDGMENT

We thank the staff of the BL19U2 beamline at the National Center for Protein Science Shanghai and Shanghai Synchrotron Radiation Facility (Shanghai, People's Republic of China) for assistance during data collection.

REFERENCES

(1) Hu, C.; Gu, F.; Tai, Z.; Yao, C.; Gong C.; Xia Q.; Gao, Y.; Gao S. Synergistic effect of reduced polypeptide micelle for co-delivery of doxorubicin and TRAIL against drug-resistance in breast cancer. *Oncotarget* **2016**, 7, 61832-61844.

(2) Warburg, O. On the Origin of Cancer Cell. *Science* **1956**, 123, 309-314.

(3) Zhai, J.; Luwor, R.B.; Ahmed, N.; Escalona, R.; Tan, F.H.; Fong, C.; Ratcliffe, J.; Scoble, J.A.; Drummond, C.J.; Tran, N. Paclitaxel-Loaded Self-Assembled Lipid Nanoparticles as Targeted Drug Delivery Systems for the Treatment of Aggressive Ovarian Cancer. *ACS Appl. Mater. Interfaces* **2018**, 10, 25174-25185.

(4) Angelova, A.; Garamus, V. M.; Angelov, B.; Tian, Z.; Li, Y.; Zou, A. Advances in structural design of lipid-based nanoparticle carriers for delivery of macromolecular drugs, phytochemicals and anti-tumor agents. *Adv. Colloid Interface Sci.* **2017**, *249*, 331-345.

(5) Shen, G.Z.; Xing, R.R.; Zhang, N.C.; Chen, J.; Ma, G.H.; Yan, X.H. Interfacial Cohesion and Assembly of Bioadhesive Molecules for Designof Long-Term Stable Hydrophobic Nanodrugs towards Effective Anticancer Therapy. *ACS Nano* **2016**, 10, 5720-5729.

(6) Abdelaziz, H.M.; Elzoghby, A.O.; Helmy, M.W.; Samaha, M.W.; Fang, J.Y.; Freag, M.S. Liquid crystalline assembly for potential combinatorial chemo-herbal drug delivery to lung cancer cells. *Int. J. Nanomedicine* **2019**, 14, 499-517.

(7) Tan, A.; Hong, L.; Du, J.D.; Boyd, B.J. Self-Assembled Nanostructured Lipid Systems: Is There a Link between Structure and Cytotoxicity? *Advanced Science* **2019**, 6, 1801223.

(8) Chen, Y.; Angelova, A.; Angelov B.; Drechsler, M.; Garamus, V. M.; Regine Willumeit-Römere, R.; Zou, A. Sterically stabilized spongosomes for multidrug delivery of anticancer nanomedicines, *J. Mater. Chem. B* **2015**, 3, 7734-7744.

(9) Thapa, R.K.; Nguyen, H.T.; Jeong, J.H.; Shin, B.S.; Ku, S.K.; Choi, H.G.; Yong, C.S.; Kim, J.O. Synergistic anticancer activity of combined histone deacetylase and proteasomal inhibitor-loaded zein nanoparticles in metastatic prostate cancers. *Nanomedicine* **2017**, 13, 885-896.

(10) Sui, J.; Cui, Y.; Cai, H.; Bian, S.; Xu, Z.; Zhou, L.; Sun, Y.; Liang, J.; Fan, Y.; Zhang, X. Synergistic chemotherapeutic effect of sorafenib-loaded pullulan-Dox conjugate nanoparticles against murine breast carcinoma. *Nanoscale* **2017**, 9, 2755-2767.

(11) Gong, X.J.; Moghaddam, M.J.; Sagnella, S.M.; Conn, C.E.; Danon, S.J.; Waddington, L.J. Drummond, C.J. , Lyotropic Liquid Crystalline Self-Assembly Material Behavior and Nanoparticulate Dispersions of a Phytanyl Pro-Drug Analogue of Capecitabine A Chemotherapy Agent. *ACS Appl. Mater. Interfaces* **2011**, 3, 1552.

(12) Thapa, R.K.; Choi, J.Y.; Gupta, B.; Ramasamy, T.; Poudel, B.K.; Ku, S.K.; Youn, Y.S.; Choi, H.G.; Yong, C.S.; Kim, J.O. Liquid crystalline nanoparticles encapsulating cisplatin and docetaxel combination for targeted therapy of breast cancer. *Biomater Sci*. **2016**, 4, 1340-1350.

(13) Freag, M.S.; Elnaggar, Y.S.; Abdelmonsif, D.A.; Abdallah, O.Y. Layer-by-layer-coated lyotropic liquid crystalline nanoparticles for active tumor targeting of rapamycin. *Nanomedicine (Lond)*. **2016**, 11, 2975-2996.

(14) Urandur, S.; Banala, V.T.; Shukla, R.P.; Mittapelly, N.; Pandey, G.; Kalleti, N.; Mitra, K. Rath, S.K.; Trivedi, R. Ramarao, P.; Mishra, P.R. Anisamide-Anchored Lyotropic Nano-Liquid Crystalline Particles with AIE Effect: A Smart Optical Beacon for Tumor Imaging and Therapy. *ACS Appl. Mater. Interfaces* **2018**, 10, 12960–12974.

(15) Bor, G.; Mat-Azmi, I.D.; Yaghmur, A. Nanomedicines for cancer therapy: current status, challenges and future prospects. *Ther. Deliv*. **2019**, 10, 113-132.

(16) Gustafsson, J.; Ljusberg-Wahren, H.; Almgren, M.; Larsson, K. Cubic lipid−water phase dispersed into submicron particles. *Langmuir* **1996**, 12, 4611−4613.

(17) Nguyen, T.H.; Hanley, T.; Porter, C.J.; Boyd, B.J. Nanostructured liquid crystalline particles provide long duration sustained-release effect for a poorly water soluble drug after oral administration. *J Control Release* **2011**, 153, 180-186.

(18) Angelov, B.; Angelova, A.; Papahadjopoulos-Sternberg, B.; Hoffmann, S.V.; Nicolas, V.;

Lesieur, S. Protein-Containing PEGylated Cubosomic Particles: Freeze-Fracture Electron Microscopy and Synchrotron Radiation Circular Dichroism Study, *J. Phys. Chem. B* **2012**, 116, 7676−7686.

(19) Zerkoune, L.; Lesieur, S.; Putaux, J.-L.; Choisnard, L.; Gèze, A.; Wouessidjewe, D.; Angelov, B.; Vebert-Nardin, C.; Doutch, J.; Angelova, A. Mesoporous self-assembled nanoparticles of biotransesterified cyclodextrins and nonlamellar lipids as carriers of water-insoluble substances, *Soft Matter* **2016**, *12*, 7539-7550.

(20) Thapa, R.K.; Choi, J.Y.; Poudel, B.K.; Hiep, T.T.; Pathak, S.; Gupta, B.; Choi, H.G.; Yong, C.S.; Kim, J.O. Multilayer-Coated Liquid Crystalline Nanoparticles for Effective Sorafenib Delivery to Hepatocellular Carcinoma. *ACS Appl. Mater. Interfaces* **2015**, 7, 20360-20368.

(21) Angelova, A.; Fajolles, C.; Hocquelet, C.; Djedaïni-Pilard, F.; Lesieur, S.; Bonnet, V.; Perly, B.; Le Bas, G.; Mauclaire, L. Physico-chemical investigation of asymmetrical peptidolipidyl-cyclodextrins. *Journal of Colloid and Interface Science* **2008**, *322*, 304-314.

(22) Clogston, J.; Caffrey, M. Controlling release from the lipidic cubic phase. Amino acids, peptides, proteins and nucleic acids. *J. Controlled Release* **2005**, 107, 97-111.

(23) Mulet, X.; Boyd, B.J.; Drummond, C.J. Advances in Drug Delivery and Medical Imaging Using Colloidal Lyotropic Liquid Crystalline Dispersions. *J. Colloid Interface Sci*. **2013**, 393, 1-20.

(24) Fong, W.K.; Negrini, R.; Vallooran, J.J.; Mezzenga, R.; Boyd, B.J. Responsive self-assembled nanostructured lipid systems for drug delivery and diagnostics. *Journal of Colloid and Interface Science* **2016**, 484, 320-339.

(25) Urandur S.; Marwaha, D.; Gautam, S.; Banala, V.T.; Sharma, M.; Mishra, P.R. Nonlamellar liquid crystals: a new paradigm for the delivery of small molecules and bio-macromolecules. *Therapeutic Delivery* **2018**, *9*, 667-689.

(26) Göke, K.; Lorenz, T.; Repanas, A.; Schneider, F.; Steiner, D.; Baumann, K.; Bunjes, H.; Dietzel, A.; Finke, J.H.;, Glasmacher, B.; Kwade, A. Novel strategies for the formulation and processing of poorly water-soluble drugs. *Eur J Pharm Biopharm.* **2018**, *126*, 40-56.

(27) Negrini, R.; Mezzenga, R. Diffusion, Molecular Separation, and Drug Delivery from Lipid Mesophases with Tunable Water Channels. *Langmuir* **2012**, 28, 16455-16462.

(28) Boyd, B.J.; Fong, W.K. Stimuli-Responsive Lipid-Based Self-Assembled Systems, In Self-Assembled Supramolecular Architectures. *John Wiley & Sons, Inc*. **2012**, pp. 257–288.

(29) Li, S.K.; Zou, Q.L.; Li, Y.X.; Yuan, C.Q.; Xing, R.R.; Yan, X.H., Smart Peptide-Based Supramolecular Photodynamic Metallo-Nanodrugs Designed by Multicomponent Coordination Self-Assembly. *J. Am. Chem. Soc.* **2018**, 140, 10794-10802.

(30) Li, Y.X.; Zou, Q.L.; Yuan, C.Q.; Li, S.K.; Xing, R.R.; Yan, X.H., Amino Acid Coordination-Driven Self-Assembly for Enhancing both Biological Stability and Tumor Accumulation of Curcumin. *Angew. Chem. Int. Ed.* **2018**, 57, 17084-17088.

(31) Salentinig, S.; Sagalowicz, L.; Glatter, O. Self-assembled structures and pKa value of oleic acid in systems of biological relevance. *Langmuir* **2010**, 26, 11670-11679.

(32) Mele, S.; Söderman, O.; Ljusberg-Wahrén, H.; Thuresson, K.; Monduzzi, M.; Nylander, T. Phase behavior in the biologically important oleic acid/sodium oleate/water system. *Chem Phys Lipids* **2018**, 211, 30-36.

(33) Negrini, R.; Fong, W.K. Boyd, B.J.; Raffaele, M. pH-responsive lyotropic liquid crystals and their potential therapeutic role in cancer treatment. *Chemical Communications* **2015**, 51, 6671-6674.

(34) Fong, W.K.; Hanley, T.L.; Thierry, B.; Hawley, A.; Boyd, B.J.; Landersdorfer, C.B.. External manipulation of nanostructure in photoresponsive lipid depot matrix to control and predict drug release in vivo. *Journal of Controlled Release* **2016**, 228, 67-73.

(35) Nazaruk, E.; Górecka, E.; Osornio, Y.M.; Landau, E.M. Bilewicz, R. Charged additives modify drug release rates from lipidic cubic phase carriers by modulating electrostatic interactions. *Journal of Electroanalytical Chemistry* **2018**, 819, 269-274.

(36) Gontsarik, M.; Yaghmur, A.; Ren, Q.; Maniura-Weber, K.; Salentinig, S. From Structure to Function: pH-Switchable Antimicrobial Nano-Self-Assemblies. *ACS Appl. Mater. Interfaces* **2019**, 11, 2821-2829.

(37) Gao, W.W.; Chan, J.M.; Farokhzad, O.C. pH-Responsive Nanoparticles for Drug Delivery. *Mol. Pharmaceutics* **2010**, 7, 1913-1920.

(38) Hruby, M.; Konak, C.; Ulbrich, K. Polymeric micellar pH-sensitive drug delivery system for doxorubicin. *J. Controlled Release* **2005**,103, 137-148.

(39) Chen, M.; Chen, R.; Wang, S. Tan, W.; Hu, Y.; Peng, X.; Wang, Y. Chemical components,

pharmacological properties, and nanoparticulate delivery systems of Brucea javanica. *Int. J. Nanomed*. **2013**, 8, 85–92.

(40) Zhang, H.; Yang, J.Y.; F. Zhou,; Wang, L.H.; Zhang, W. Seed Oil of Brucea javanica Induces Apoptotic Death of Acute Myeloid Leukemia Cells via Both the Death Receptors and The Mitochondrial-Related Pathways. *Evidence-Based Complementary and Alternative Medicine* **2011**, 5, 965016.

(41) Jiang, X.; Zeng, Y.Y.; Di, J.F.; He, X.H.; Feng, Z.; Zeng, S.; Chen, W.X. Preliminary studies on the effects of Brucea Javanica emulsion on HPV positive tumor cells form laryngeal papilloma in child. *Journal of Jinan University (Medicine Edition)* **2004**, 25, 408–412.

(42) Yin, X.J.; Luan, H.Z.; An, C.L.; Wang, X.L.; Bing, Y.Y.; Wang, X.N. Inhibitory effect of Brucea javanica oil emulsion against cervical cancer cell line Hela and its mechanism. *Chinese Journal of Cancer Biotherapy* **2008**, 15, 393–395.

(43) Han, F.; Cai, D.; Wu, X.; Zhai, X. Wang, L. Research progress of Brucea javanica antitumor mechanism, *Journal of Modern Oncology* **2013**, 21, 669–671.

(44) Chen, D.; Chen, P.; Zhu, M. Reverse Effect of Brucea Javanica Oil Emulsion on Drug Resistant Human Ovarian Carcinoma Cells A2780/DDP. *Journal of Emergency in Traditional Chinese Medicine* **2009**, 18,598–599.

(45) Su, S.Y. Treatment of lung cancer with brainmetastasis using an intravenous drip of a 10% emulsion of Brucea javanica seminal oil. *Chinese Journal of Integrative Medicine* **1985**, 5, 86–88.

(46) Ma, L.; Zhang, Y. N.; Effects of seminal oil emulsion of Brucea javanica on apoptosis and apoptosis-related genes in human hepatocellular carcinoma cells. *World Chinese Journal of Digestology*. **2004**, 12, 559–562.

(47) He, D.L.; Nan, X.Y.; Liu, W.S. The antitumor effect of 10% Brucea Javanica oil emulsion on prostate cancer cells. *Journal of Clinical Urology* **1994**, 9, 60–62.

(48) Lv, W.; Zhao, S.; Yu, H.; Li, N.; Garamus, V.M.; Chen, Y.; Yin, P.; Zhang, R.; Gong, Y.; Zou, A. *Brucea javanica* oil-loaded nanostructure lipid carriers (BJO NLCs): Preparation, characterization and in vitro evaluation. *Colloids and Surfaces A: Physicochemical and Engineering Aspects* **2016**, 504, 312-319.

(49) Zhu, C.; Liu, X.; Li, G. Effect of *Brucea javanica* oil emulsion combined with Adriamycin for refractory malignant pleural effusion. *Applied Journal of General Practice* **2007**, 5, 871.

(50) Chabner, B.A.; Amrein, P.C.; Druker, B.J.; Michaelson, M.D.; Mitsiades, C.S.; Goss, P.E.; Ryan, D.P.; Ramachandra, S.; Richardson, P.G.; Supka, J.G.; Wilson, W.H. Antineoplastic agents. In Brunton, L.L. Lazo, J.S. Parker, K.L. (Eds.), Goodman & Gilman's The Pharmacological Basis of Therapeutics. Mc Graw Hill, New York, **2006**, p. 1357–1359.

(51) Brandenburg, K.; Richter, W.; Koch, M.H.; Meyer, H.W.; Seydel, U. Characterization of the nonlamellar cubic and HII structures of lipid A from Salmonella enterica serovar Minnesota by X-ray diffraction and freeze-fracture electron microscopy. *Chemistry and Physics of Lipids* **1998**, 91(1):53-69.

(52) de Campo, L.; Yaghmur, A.; Sagalowicz, L.; Leser, M. E.; Watzke, H.; Glatter, O. Reversible phase transitions in emulsified nanostructured lipid systems. *Langmuir* **2004**, 20, 5254−5261.

(53) Angelov, B.; Angelova, A.; Mutafchieva, R.; Lesieur, S.; Vainio,U.; Garamus, V. M.; Jensen, G. V.; Pedersen, J. S. SAXS investigation of a cubic to a sponge (L3) phase transition in self-assembled lipid nanocarriers. *Phys. Chem. Chem. Phys*. **2011**, 13, 3073−3081.

(54) Chen, L.Q.; Pagel, M.D. Evaluating pH in the Extracellular Tumor Microenvironment Using CEST MRI and Other Imaging Methods. *Adv Radiol*. **2015**; 2015, 206405.

(55) Guo, C.; Wang, J.; Cao, F.; Lee, R.J.; Zhai, G. Lyotropic liquid crystal systems in drug delivery. *Drug Discovery Today* **2010**, 15, 1032.

(56) Phan, S.; Fong, W.K.; Kirby, N.; Hanley, T.; Boyd, B.J.; Evaluating the link between self-assembled mesophase structure and drug release. *Int J Pharm* **2011**, 421(1), 176-182.

(57) Sackmann, E. Supported membranes: Scientific and practical applications. *Science* **1996**, 271, 43−48.

(58) Angelova, A.; Ringard-Lefebvre, C.; Baszkin, A. Drug-cyclodextrin association constants determined by surface tension and surface pressure measurements. II. Sequestration of water insoluble drugs from the air/water interface: Retinol/beta-cyclodextrin system. *J. Colloid Interface Sci.* **1999**, *212*, 280-285.

(59) Richter, R.P.; Bérat, R.; Brisson, A.R. Formation of Solid- Supported Lipid Bilayers: An

Integrated View. *Langmuir* **2006**, 22, 3497−3505.

(60) Maximino, M.D.; Constantino, C.J.L.; Oliveira, O.N.; Alessio, P. Synergy in the interaction of amoxicillin and methylene blue with dipalmitoyl phosphatidyl choline (DPPC) monolayers. *Applied Surface Science* **2019**, 476, 493-500.

(61) Jabłonowska, E.; Nazaruk, E.; Matyszewska, D.; Speziale, C.; Mezzenga, R.; Landau, E.M.; Bilewicz, R. Interactions of Lipidic Cubic Phase Nanoparticles with Lipid Membranes. *Langmuir* **2016**, 32, 9640-9648.

(62) Vandoolaeghe, P.; Tiberg, F.; Nylander, T. Interfacial Behaviorof Cubic Liquid Crystalline Nanoparticles at Hydrophilic and Hydrophobic Surfaces. *Langmuir* **2006**, 22, 9169−9174.

(63) Vandoolaeghe, P.; Rennie, A. R.; Campbell, R. A.; Nylander, T.Neutron Reflectivity Studies of the Interaction of Cubic-PhaseNanoparticles with Phospholipid Bilayers of Different Coverage. *Langmuir* **2009**, 25, 4009−4020.

(64) Peetla, C.; Stine, A.; Labhasetwar, V. Biophysical interactions with model lipid membranes: applications in drug discovery and drug delivery. *Mol. Pharm.*, **2009**, 6, 1264-1276.

Table of Contents (TOC)